

The effect of ultra-violet photon pumping of H₂ in dust-deficient protoplanetary disks

AYANO KOMAKI,¹ RIOUHEI NAKATANI,² ROLF KUIPER,³ AND NAOKI YOSHIDA^{1,4,5}

¹*Department of Physics, The University of Tokyo, 7-3-1 Hongo, Bunkyo, Tokyo 113-0033, Japan*

²*RIKEN Cluster for Pioneering Research, 2-1 Hirosawa, Wako-shi, Saitama 351-0198, Japan*

³*Zentrum für Astronomie der Universität Heidelberg, Institut für Theoretische Astrophysik, Albert-Ueberle-Straße 2, 69120 Heidelberg, Germany*

⁴*Kavli Institute for the Physics and Mathematics of the Universe (WPI), UT Institute for Advanced Study, The University of Tokyo, Kashiwa, Chiba 277-8583, Japan*

⁵*Research Center for the Early Universe (RESCEU), School of Science, The University of Tokyo, 7-3-1 Hongo, Bunkyo, Tokyo 113-0033, Japan*

(Received; Revised; Accepted)

Submitted to ApJ

ABSTRACT

We perform radiation hydrodynamics simulations to study the structure and evolution of a protoplanetary disk. Ultraviolet and X-ray radiation from the host star heats the disk surface, where H₂ pumping also operates efficiently. We run a set of simulations with varying the amount of dust grains, or the dust-to-gas mass ratio, which determines the relative importance between photoelectric heating and H₂ pumping. We show that H₂ pumping and X-ray heating contributes stronger to the mass-loss of the disk if the dust-to-gas mass ratio is $\mathcal{D} \leq 10^{-3}$. In such dust-deficient disks, H₂ pumping enhances photoevaporation from the inner disk region and shapes the disk mass-loss profile. The long-term disk dispersal process may be affected by the ultra-violet H₂ pumping effect.

1. INTRODUCTION

Circumstellar disks around newly born stars evolve to be protoplanetary disks (PPDs) where planets are formed. Recent interferometric observations revealed directly the shape and the chemical structure of PPDs (Walsh et al. 2015; Ansdell et al. 2016; Johnston et al. 2020). Near infrared observations also show that the disk fraction in a star-forming region decreases as the age of the central star, suggesting that PPDs disappear in 3–6 Myr (e.g., Haisch et al. 2001; Meyer et al. 2007; Hernández et al. 2007; Mamajek 2009; Bayo et al. 2012; Ribas et al. 2014).

Photoevaporation is suggested to be an important disk dispersal mechanism. High-energy photons such as far-ultraviolet (FUV; $6\text{ eV} \lesssim h\nu < 13.6\text{ eV}$), extreme-ultraviolet (EUV; $13.6\text{ eV} \lesssim h\nu \lesssim 100\text{ eV}$), and X-ray ($100\text{ eV} \lesssim h\nu \lesssim 10\text{ keV}$) emitted from the central star heat a large portion of a PPD through various radiative and photo-chemical processes. It is generally found that EUV photons are mainly absorbed by abundant neutral hydrogen close to the central star, while FUV and

X-ray photons penetrate deep into the disk, to drive dense photoevaporative flows (e.g., Richling & Yorke 2000; Ercolano et al. 2009; Gorti & Hollenbach 2009). FUV photons are the cause of the photoelectric effect on dust grains in the disk, whereas EUV and X-ray do through ionization of hydrogen, helium, and other heavy elements. These processes altogether raise the gas temperature of the disk surface and generate photoevaporative flows.

PPDs typically have a complicated, multi-layer structure in which various chemical species exist in different regions. It has been suggested by both observations and numerical simulations that H₂ molecules in the neutral regions absorb the radiation from the central star and affect the observed spectral energy distribution (Herzceg et al. 2004; Nomura & Millar 2005; Schindhelm et al. 2012). The so-called UV pumping of H₂ molecules (H₂ pumping hereafter) can be an important heating process in the region where a substantial amount of H₂ molecules are continuously formed and destroyed. The net heating process can affect the thermal structure of a photoevaporating disk with a sufficiently high FUV (Wang & Goodman 2017). H₂ pumping is a two-step process that Lyman-Werner photons (LW photons;

$11.2\text{ eV} \lesssim h\nu < 13.6\text{ eV}$) excite H_2 molecules to the electronically excited state followed by de-excitation to the vibrationally excited state of the ground electronic state (Tielens & Hollenbach 1985). Collisional de-excitation to the vibrationally ground state results in heating the gas by distributing the de-excitation energy to the surrounding atoms and molecules. Note that, while the FUV photoelectric heating rate roughly scales with the local amount of small grains, H_2 pumping may operate even in regions with little dust content.

The disk dust properties are characterised by the dust-to-gas mass ratio and the size distribution. Since these quantities may be inhomogeneous in time and in space within the disk, the relative importance of the heating processes can also significantly change according to the disk evolution. Dust grains undergo physical processing during the disk evolution. Numerical calculations show that small dust grains entrain photoevaporative flows (Hutchison et al. 2016). Dust settling may occur in PPDs, as inferred from infrared observations and SED modelling (D’Alessio et al. 1999, 2006; Grant et al. 2018). Grown dust can move inward by radial drift, likely making the dust disk radius apparently smaller than the gas disk radius, as suggested by ALMA observations (de Gregorio-Monsalvo et al. 2013; Ansdell et al. 2018). Millimeter observations suggest that the dust mass decreases as the system age increases (Mathews et al. 2012; Ansdell et al. 2016; Pascucci et al. 2016; Ansdell et al. 2017). Dust sedimentation can reduce the local dust-to-gas mass ratio of the disk surface significantly. The total dust-to-gas mass ratio of a disk likely varies through its evolutionary phases. Dust growth changes the total surface area of grains. It strongly impacts on the disk opacity, photoelectric heating, dust-gas collision, and formation of molecules, meaning that dust growth does impact on photoevaporation and disk lifetimes (Gorti et al. 2015). Although the actual dust-to-gas mass ratio is uncertain, overall it appears meaningful to study the evolution of PPDs with considering a wide range of dust-to-gas mass ratio.

In this paper, we perform hydrodynamics simulations to study the disk photoevaporation and the dispersal. H_2 pumping is incorporated to closely examine the effect of H_2 pumping on the disk temperature. We vary the dust-to-gas mass ratio of the disk, \mathcal{D} , in the range of 10^{-8} – 10^{-1} to study how the disk thermochemical distribution changes. Finally, we examine if H_2 pumping is an important heating process around a massive star. We increase the stellar mass from $M_* = 1 M_\odot$ to $M_* = 7 M_\odot$ and also increase the central luminosity at the same time. We explain our methods in Section 2. We

show our results in Section 3 and discussions in Section 4. In Section 5 we summarize.

2. NUMERICAL SIMULATIONS

We perform disk photoevaporation simulations including hydrodynamics, radiative transfer and non-equilibrium chemistry in a coupled and self-consistent manner. We use the open source code PLUTO (Mignone et al. 2007) suitably modified for simulations of PPDs. The details of the implemented physics are found in Nakatani et al. (2018a,b) and Komaki et al. (2021). We assume the disk is axisymmetric around the rotational axis and adopt the 2D spherical coordinates (r, θ) . We consider three components of the gas velocity, $\mathbf{v} = (v_r, v_\theta, v_\phi)$.

We first run our fiducial case, where the stellar mass $M_* = 1 M_\odot$ and $\mathcal{D} = 10^{-2}$, with a detailed treatment of H_2 pumping. In the case of $\mathcal{D} = 10^{-2}$, we calculate the dust temperature in the same way as Komaki et al. (2021), where we calculate and tabulate the dust temperature as a function of the distance from the central star and the column density, based on the results of more costly radiative transfer calculations. In our runs with other dust-to-gas mass ratios, we solve the dust temperature in a self-consistent manner by incorporating both the direct and diffuse radiation. We perform ray-tracing for the direct component and adopt the flux-limited-diffusion (FLD) approximation for the diffused component (Kuiper et al. 2010; Kuiper & Klessen 2013; Kuiper et al. 2020).

We incorporate EUV/X-ray photoionization heating, FUV photoelectric heating (Bakes & Tielens 1994), and heating by H_2 photodissociation and by H_2 pumping. We also incorporate dust-gas collisional cooling (Yorke & Welz 1996), fine-structure cooling of C II and O I (Hollenbach & McKee 1989; Osterbrock 1989; Santoro & Shull 2006), molecular line cooling of H_2 and CO (Galli & Palla 1998; Omukai et al. 2010), hydrogen Lyman α line cooling (Anninos et al. 1997), and radiative recombination cooling (Spitzer 1978) as cooling sources.

The chemical reaction network follows the abundances of eleven chemical species: H I, H II, H^- , He I, H_2 , H_2^+ , H_2^* , CO, O I, C II and electrons in the run with $M_* = 1 M_\odot$, $\mathcal{D} = 10^{-2}$. We denote the vibrationally excited state of H_2 ($v = 6$) as H_2^* and treat as a distinct chemical species (Tielens & Hollenbach 1985). H_2 has hundreds of excited states, but the pseudo-level of $v = 6$ approximately represents the excited levels altogether, which then reduces the computational cost significantly. We also use the pseudo-level of H_2^* to study the effect of H_2 pumping on the disk thermal structure. We assume that C I is quickly ionized to become C II after the

dissociation of CO (Nelson & Langer 1997; Richling & Yorke 2000).

H₂ pumping is the process where LW photons excite H₂ molecule to the electronically excited state and then de-excite to a vibrationally excited state of the ground electronic state (Tielens & Hollenbach 1985). In the run with $M_* = 1 M_\odot$, $\mathcal{D} = 10^{-2}$, we incorporate H₂* to calculate both the excitation rate and the de-excitation rate. We calculate the H₂ pumping rate, R_{pump} as

$$R_{\text{pump}} = 3.4 \times 10^{-10} \beta G_0 e^{-2.5 A_v} \text{ s}^{-1},$$

following Tielens & Hollenbach (1985). We define β , G_0 and A_v as the shielding factor, the intensity of the incident FUV field and the visual extinction respectively. We determine the shielding factor by H₂ following Draine & Bertoldi (1996). The vibrationally excited H₂ molecules de-excite and fluoresce. We incorporate the collisional de-excitation by H I or H₂ as the de-excitation reactions. We also consider the direct dissociation of H₂* by FUV radiation and by spontaneous radiation (Tielens & Hollenbach 1985). We define $k_{\text{de}}(\text{H})$, $k_{\text{de}}(\text{H}_2)$, R_{de} , $A(\text{H}_2^*)$ as the reaction rates by the collision with H I, the collision with H₂, the direct dissociation by FUV radiation and the spontaneous radiation respectively. The reaction rates are written as

$$\begin{aligned} k_{\text{de}}(\text{H}) &\simeq 1.8 \times 10^{-13} \text{ cm}^3 \text{ s}^{-1} \\ &\times \left(\frac{T_{\text{gas}}}{\text{K}} \right)^{1/2} \exp \left(-\frac{1000 \text{ K}}{T_{\text{gas}}} \right) \\ k_{\text{de}}(\text{H}_2) &\simeq 2.3 \times 10^{-13} \text{ cm}^3 \text{ s}^{-1} \\ &\times \left(\frac{T_{\text{gas}}}{\text{K}} \right)^{1/2} \exp \left(-\frac{1800 \text{ K}}{(T_{\text{gas}} + 1200 \text{ K})} \right) \\ R_{\text{de}} &= 10^{-11} \beta G_0 e^{-2.5 A_v} \text{ s}^{-1} \\ A(\text{H}_2^*) &= 2.0 \times 10^{-7} \text{ s}^{-1}, \end{aligned}$$

where T_{gas} represents the gas temperature. We follow Wang & Goodman (2017) to obtain reaction rates. Each collisional de-excitation process deposits 2.6 eV and each de-excitation by direct FUV radiation deposits 0.4 eV (Tielens & Hollenbach 1985).

We explicitly treat H₂* as a distinct chemical species in the fiducial run where $M_* = 1 M_\odot$ and $\mathcal{D} = 10^{-2}$. For the other runs, we calculate H₂ pumping without explicitly including the excited molecular hydrogen, as in Röllig et al. (2006), Gressel et al. (2020) and Nakatani et al. (2021):

$$\frac{de}{dt} = n_{\text{H}_2} \frac{\chi P_{\text{tot}} \Delta E_{\text{eff}}}{1 + [A_{\text{eff}} + \chi D_{\text{eff}}]/[\gamma_{\text{eff}} n]}, \quad (1)$$

where χ is the FUV radiation intensity in units of the local interstellar radiation field, P_{tot} and n are the formation rate of H₂* and the particle number density,

respectively. The coefficients ΔE_{eff} , A_{eff} , D_{eff} , γ_{eff} express the average excitation energy, the effective spontaneous emission rate, the effective dissociation rate, and the effective collisional de-excitation rate assuming that molecular hydrogen has two levels, the ground state and the pseudo-excited level. We set $P_{\text{tot}} \Delta E_{\text{eff}} = 9.4 \times 10^{-22} \text{ erg s}^{-1}$, $A_{\text{eff}} = 1.9 \times 10^{-6} \text{ s}^{-1}$, $D_{\text{eff}} = 4.7 \times 10^{-10} \text{ s}^{-1}$ and $\gamma_{\text{eff}} = 5.4 \times 10^{-13} \sqrt{T_{\text{gas}}} \text{ s}^{-1} \text{ cm}^{-3}$ following Röllig et al. (2006) and Gressel et al. (2020). We have checked that using this formula does not change the resulting mass-loss profiles. It can reduce the computational time by ~ 1.5 times compared to the run without H₂*.

The size distribution of dust grains is assumed to follow $dn(a) \propto a^{-3.5} da$ with a denoting dust radii (Draine & Lee 1984). Bakes & Tielens (1994) show that small grains are crucial for efficient photoelectric heating. In practice, dust dynamics such as sedimentation, radial drift and/or turbulent mixing can change the dust distribution across the disk. However, for simplicity, we set the dust-to-gas mass ratio to constant throughout the computational domain. The underlying assumption is that the dust grains responsible for photoelectric heating are well mixed within the gas so that we treat the mixture of dust and gas as a single fluid. We perform a set of simulations with different constant values of the dust-to-gas mass ratio. Note that the dust amount near the disk surface, where photoevaporative flows are launched, critically determines the disk mass-loss rate. We perform disk evolution simulations with varying the dust-to-gas mass ratio for the disk \mathcal{D} in the range of 10^{-8} – 10^{-1} as a parameter to examine how the effective heating and cooling processes vary with \mathcal{D} . In our simulations, the dust opacity, photoelectric heating rate, dust-gas collisional cooling rate, the rate of H₂ formation catalyzed by grains are scaled with $(\mathcal{D}/0.01)$. Our fiducial dust-to-gas mass ratio is $\mathcal{D} = 10^{-2}$, which corresponds to the local ISM value. The gas-phase elemental abundance of carbon is set to $y_{\text{C}} = 0.927 \times 10^{-4}$ and that of oxygen to $y_{\text{O}} = 3.568 \times 10^{-4}$ (Pollack et al. 1994). We assume y_{C} and y_{O} to be constant even when we set different \mathcal{D} .

We take into account FUV, EUV and X-ray radiations as the high-energy radiation from the central star. As in our previous paper Komaki et al. (2021), we choose the FUV, EUV and X-ray luminosities, ϕ_{EUV} , L_{FUV} , L_{X} , following Table 1 in Gorti & Hollenbach (2009), which shows typical 1 Myr pre-main sequence star luminosities.

We define the computational domain of the polar angle to $[0, \pi/2]$, and the radial coordinate to $[0.1r_g, 20r_g]$. The gravitational radius r_g for a fully ionized gas with

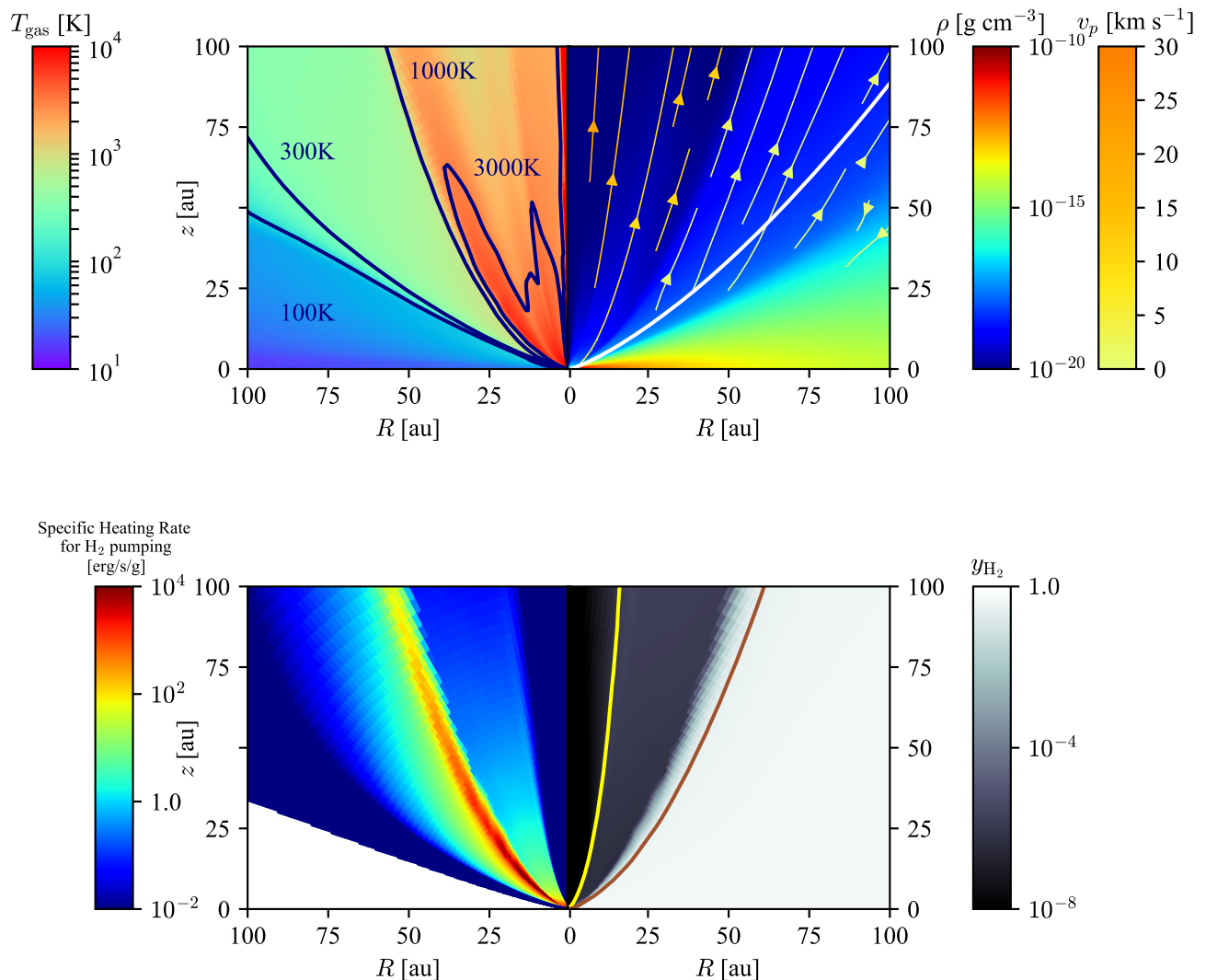


Figure 1. (top) The time-averaged disk structure of the run incorporating H_2 pumping. The color map on the left portion shows the gas temperature, T_{gas} , and the right portion shows the density distribution, ρ . The white line shows the location of the base, which satisfies $N_{\text{H}_2} = 10^{20} \text{ cm}^{-2}$. The navy contour lines on the left side represent where the gas temperature is 100 K, 300 K, 1000 K, and 3000 K. The streamline represents the poloidal velocity of the gas, which is defined as $v_p = \sqrt{v_r^2 + v_\theta^2}$. For clarity, we omit to plot the streamlines where the velocity is less than 0.1 km s^{-1} , which are mostly seen in the optically thick disk region. (bottom) The time-averaged disk chemical structure of the run incorporating H_2 pumping. The color map on the left portion shows the specific heating rate for H_2 pumping. The right portion shows the abundance of H_2 . The right portion also shows the distribution of H-bearing species. The yellow line on the right side represents the ionization front where the abundance of H II is 0.5, and the brown line indicates the dissociation front where the abundance of H_2 is 0.25.

$T_{\text{gas}} = 10^4 \text{ K}$ is

$$r_g = \frac{GM_*}{(10 \text{ km s}^{-1})^2} \simeq 8.87 \text{ au} \left(\frac{M_*}{1 M_\odot} \right),$$

where G is the gravitational constant. The gravitational radius sets the estimate of the effective boundary where the photoevaporative flows can escape out of the potential well of the host star. However hydrodynamics sim-

ulations show that the photoevaporative flows are also excited inside the gravitational radius from the critical radius $\sim 0.2 r_g$ (Liffman 2003; Font et al. 2004). Motivated by findings, we set the computational range to include the region inside the gravitational radius. We use r_g as a reference physical length scale in this paper.

We start our simulations setting the initial disk condition to be a 1 million year system, when the mass loss by

accretion becomes lower (Clarke et al. 2001; Alexander et al. 2006; Owen et al. 2010; Suzuki et al. 2016; Kunitomo et al. 2020). We assume that the disk mass, M_{disk} , is 3% of the central stellar mass (Andrews & Williams 2005). We assume the initial surface density profile, Σ and the initial temperature distribution, T_{ini} , as Komaki et al. (2021), to be

$$\begin{aligned}\Sigma(R) &= 27.1 \text{ g cm}^{-2} \times (R/r_g)^{-1} \\ T_{\text{ini}} &= 100 \text{ K} \times (R/0.1r_g)^{-1/2}.\end{aligned}$$

We run the simulations for $8.4 \times 10^3 (M_*/M_\odot)$ yr. This is 10 times of the gas Kepler rotational period around the central star at $r = r_g$ and this is long enough for the time-averaged mass-loss to converge.

3. RESULTS

In this section, we present the results of our simulations. We first describe the effect of H_2 pumping on the temperature and the chemical structure in the run with $M_* = 1 M_\odot$ and $\mathcal{D} = 10^{-2}$ in Section 3.1. We then calculate the mass-loss rate of this run in Section 3.2. Finally in Section 3.3, we describe how the disk thermal structure changes when varying the dust-to-gas mass ratio.

3.1. Thermochemical Structure

Figure 1 shows the time-averaged snapshot of the simulation with $M_* = 1 M_\odot$ and $\mathcal{D} = 10^{-2}$ and with incorporating H_2^* and H_2 pumping. To make this plot, we average the outputs from 840 yr to 8400 yr to avoid the initial transient and to smooth out (temporarily) fluctuating features. Photoevaporative flows are launched from the surface of the disk, where the column density satisfies $N_{\text{H}_2} \approx 10^{20} \text{ cm}^{-2}$ (white line in the top panel). We define this surface as the base of the photoevaporative flows.

EUV radiation heats the gas near the central star and at high latitudes, shaping the polar H II region where $y_{\text{HII}} > 0.5$. The outgoing gas cools by adiabatic cooling and has a temperature of $T_{\text{gas}} \sim 3000 \text{ K}$.

The bottom portion of Figure 1 shows the H_2 pumping heating rate $\Gamma_{\text{H}_2^*}$ and also the molecular fraction y_{H_2} . The H_2^* is most abundant near the dissociation front with a number fraction ~ 0.04 , where $\Gamma_{\text{H}_2^*}$ reaches $\sim 10^4 \text{ erg s}^{-1} \text{ g}^{-1}$. We note that the H_2 dissociation front locates at a lower polar angle than the base.

In the dense inner region at $r \lesssim 30 \text{ au}$, H_2^* molecules get de-excited mainly by collisions with H I. There, the gas is largely heated by this H_2 pumping process. The critical density for H_2^* spontaneous radiation is $\rho_c \simeq 5.0 \times 10^{-20} \text{ g cm}^{-3}$ assuming $T_{\text{gas}} = 3000 \text{ K}$. In our simulation, the density at $r \gtrsim 30 \text{ au}$ is lower than ρ_c , and

thus the spontaneous radiation primarily de-excites the H_2^* molecules there, and the resulting gas heating rate is small. We note that, in our simulations, the timescale for H_2^* de-excitation is shorter than the local hydrodynamical timescale by a factor of $\sim 10^2$, so the H_2^* molecules almost immediately get de-excited at the location where they are excited by the incident radiation.

We have run an additional simulation that does not explicitly treat H_2^* molecules. By comparing the outputs, we find that the resulting temperature structure is almost identical in all regions. This result is expected from the shorter timescales of H_2^* -involved (photo)chemical processes than the local dynamical timescale. We thus confirm that it is sufficient to implement the effect of H_2 pumping by considering its heating rate using Equation (1).

3.2. The Mass-loss Rate

The disk gas is heated by the radiation from the central star, and photoevaporative flows are launched from the disk. The disk mass-loss rate is determined by the heating process around the base. In our fiducial run, FUV photoelectric heating is the main heating source at the base, and its rate is greater than the heating rate of H_2 pumping by a factor of $\sim 10^3$ throughout the base. The resulting temperature distribution is almost the same as in the run without H_2 pumping at the base, indicating that the photoevaporative flows are driven mainly by FUV photoelectric heating.

We use the simulation outputs to calculate the mass-loss rate

$$\dot{M} = \int_{S, \eta > 0} \rho \mathbf{v} \cdot d\mathbf{S}, \quad (2)$$

where $d\mathbf{S}$ represents the spherical surface unit area at $r = 100 \text{ au}$. We define η as the Bernoulli function given by

$$\eta = \frac{1}{2}v_p^2 + \frac{1}{2}v_\phi^2 + \frac{\gamma}{\gamma - 1}c_s^2 - \frac{GM_*}{r}.$$

We define $v_p = \sqrt{v_r^2 + v_\theta^2}$ as the poloidal velocity, γ as the specific heat ratio, and c_s as the sound velocity. We assume that only the gas satisfying $\eta > 0$ has sufficient mechanical energy to escape from the system eventually.

The mass-loss rate slightly fluctuates in time mainly because of spurious reflection of subsonic gas at the outer computational boundary. The averaged mass-loss rate (from 840 yr to 8400 yr) is

$$\dot{M} = 2.7 \times 10^{-9} M_\odot \text{ yr}^{-1}.$$

The magnitude of the fluctuation is from -13% to $+10\%$ compared to the averaged value. The mass-loss rate with H_2 pumping is almost the same within the fluctuation

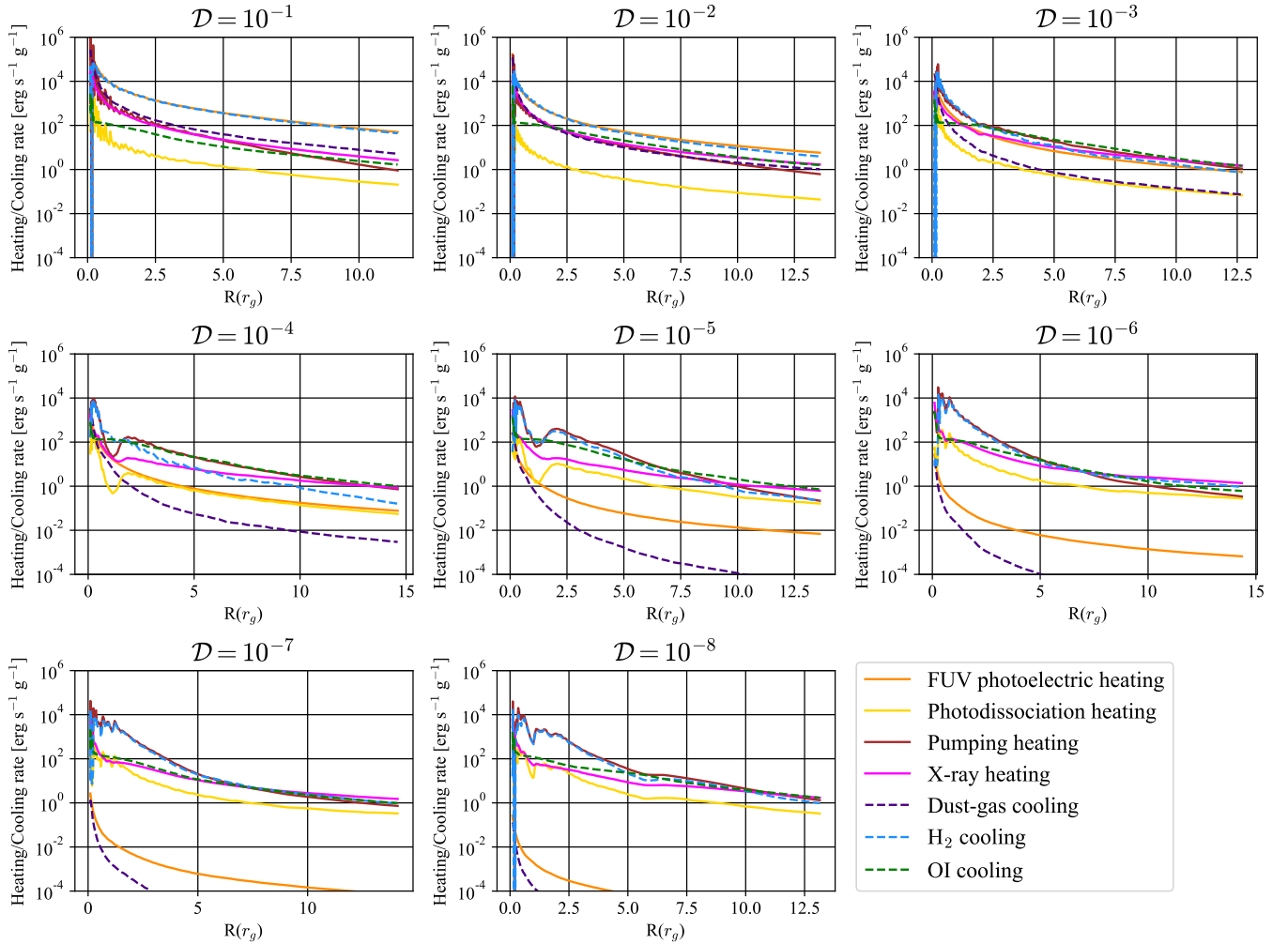


Figure 2. The time-averaged specific heating and cooling rates measured at the base in our runs with different \mathcal{D} . The solid lines show FUV photoelectric heating (orange), H_2 photodissociation heating (yellow), H_2 pumping heating (brown), and X-ray heating (magenta). The dotted lines are for dust-gas collisional cooling (purple), H_2 cooling (cyan), and O I cooling (green).

as that without H_2 pumping ($\dot{M} = 2.6 \times 10^{-9} M_{\odot} \text{ yr}^{-1}$). This is again because H_2 pumping heats the gas mainly in the vicinity of the H_2 dissociation front and does not affect the temperature structure in the photoelectric-heated region. Hence, the effect of H_2 pumping on driving photoevaporative flows is limited if H_2 -rich flow is excited by photoelectric heating.

3.3. Dependence on the Dust-to-Gas Mass Ratio

We perform a series of photoevaporation simulations with varying the dust-to-gas ratio in the range $\mathcal{D} = 10^{-8}$ – 10^{-1} .

Figure 2 shows the specific heating and cooling rates at the base in each simulation. In the case of $\mathcal{D} = 10^{-1}$, since the dust optical depth is high, FUV photons cannot deeply penetrate into the disk compared to the fiducial case ($\mathcal{D} = 10^{-2}$). Photoevaporation is caused by FUV photoelectric heating at $N_{\text{H}_2} = 10^{19} \text{ cm}^{-2}$, which

is one order of magnitude lower than the $\mathcal{D} = 10^{-2}$ case. (We define this surface as the base for this run.) The mass-loss rate decreases because of the lower base density (Figure 3).

The FUV photoelectric heating rate approximately follows $\Gamma_{\text{FUV}} \propto \mathcal{D}$ at the base. For $\mathcal{D} = 10^{-3}$, it gets lower to be comparable to heating rates for X-ray heating and H_2 pumping. The temperature of the H_2 region can not get sufficiently high to have $\eta > 0$. It is in contrast to the fiducial run where molecular flow is observed. The mass-loss rate is lower than that of the fiducial run accordingly.

For $\mathcal{D} = 10^{-4}$ – 10^{-8} , the FUV photoelectric heating is ineffective, and the thermochemical structure differs from the higher- \mathcal{D} runs. EUV photons heat the gas at high latitudes, whereas X-ray heating is dominant in the H I region instead of FUV photoelectric heating. The gas temperature is lowered to 300 K by adiabatic cooling

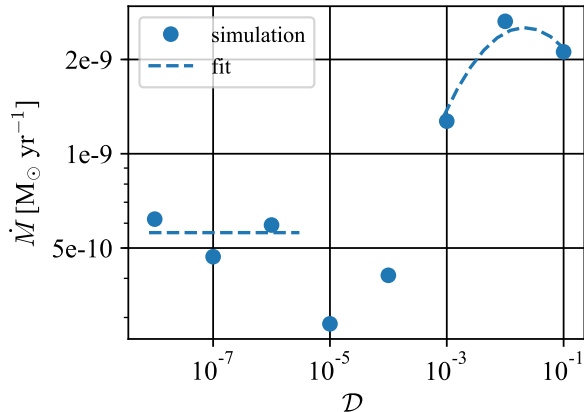


Figure 3. The time-averaged mass-loss rate for each dust-to-gas mass ratio. The blue dots represent the simulation results. The dotted line is a fit.

and O I line emission there. H₂ pumping is generally dominant only near the dissociation front, and the other H₂ region is heated by X-ray up to $N_{\text{H}} \sim 10^{22} \text{ cm}^{-2}$. Figure 2 shows the specific heating and cooling rates along the base. The relative contributions of the heating processes vary with the distance from the host star. H₂ pumping and X-ray are dominant at the radii inner and outer than $7\text{--}12r_{\text{g}}$, respectively. The inner regions are favorable for H₂ pumping since the density exceeds the critical value. The gas temperature is 200–300 K in the molecular region at $r = 10r_{\text{g}}$. It is lower by a factor of two than would have been achieved by photoelectric heating. The same is true at other radii, and thus the $\eta = 0$ boundary is present at an order of magnitude smaller column density, $N_{\text{H}_2} = 10^{19} \text{ cm}^{-2}$, than the $\mathcal{D} = 10^{-2}$ case. The flow accordingly has a low density. It results in the significant decrease in the mass-loss rate compared to the $\mathcal{D} \geq 10^{-3}$ runs (see Figure 3).

In order to extract the contribution of EUV-driven flows from the total mass-loss rates in the low- \mathcal{D} cases, we count only the mass flux of the ionized outflows ($y_{\text{HII}} \geq 0.5$) using Eq. 2. The mass-loss rates of the ionized gas are found to be roughly an order of magnitude smaller than the total, meaning that the contribution of EUV-driven flows is limited. This small contribution is mainly due to the fact that H₂ pumping increases the local scale height of the neutral gas at the innermost radii, and the vertically extended gas shields EUV that would otherwise have reached the outer radii. As a result, the H II region is confined within the conical volume at low polar angle.

The total mass-loss rates are measured in the same manner as in Section 3.2 and are fitted as a function of

\mathcal{D} . We change the fitting functions at $\mathcal{D} = 10^{-3}$, where the main heating process alternates. We get

$$\dot{M} = \begin{cases} 1.0 \times 10^{-9} \times 10^{-0.15\mathcal{D}^2 - 0.49\mathcal{D}} \text{ M}_{\odot} \text{ yr}^{-1} & (\mathcal{D} \geq 10^{-3}) \\ 5.6 \times 10^{-10} \text{ M}_{\odot} \text{ yr}^{-1} & (\mathcal{D} \leq 10^{-5}) \end{cases}$$

For $\mathcal{D} = 10^{-6} - 10^{-8}$, the mass-loss rate converges to the constant value. Since the abundance of H₂ does not strongly depend on the already small dust amount, we expect that the mass-loss rate remains constant towards even lower \mathcal{D} than shown in Figure 3.

Nakatani et al. (2018b) investigated the dependence of the mass-loss rate on the gas metallicity Z . They varied Z with setting the dust-to-gas mass ratio as $\mathcal{D} = 0.01 \times (Z/Z_{\odot})$. The gas-phase elemental abundances of metals are also scaled in proportion to (Z/Z_{\odot}) . On the other hand, we fix the gas-phase elemental abundances of carbon and oxygen constant regardless of \mathcal{D} in the present study. Our run with $\mathcal{D} = 10^{-2}$ corresponds to the $Z/Z_{\odot} = 1$ case of Nakatani et al. (2018b), which assumes ~ 10 times higher luminosities for FUV and EUV, and ~ 2.5 times higher X-ray luminosity. The overall stronger radiation yields a higher mass-loss rates in all the metallicity range. The difference between the low- Z runs of Nakatani et al. (2018b) and our low- \mathcal{D} runs appears in the major cooling process. For example, with small \mathcal{D} , O I line cooling is more effective than dust-gas collisional cooling, which has not been observed in Nakatani et al. (2018b).

4. DISCUSSION

While the results presented in the previous section have a variety of interesting implications, there are still uncertainties originating from the model assumptions. In this section, we further discuss possible variations of our results and show caveats.

4.1. Dust Evolution

It is expected that dust sedimentation causes the local dust-to-gas mass ratio to vary in the vertical direction. Dust grains can also drift radially toward the inner region. In the present study, we set the dust-to-gas mass ratio \mathcal{D} as a convenient parameter to quantify and examine the effect of dust abundance on disk photoevaporation. We have shown that the mass-loss rate and the mass-loss profile change sensitively depending on \mathcal{D} .

Infrared and millimeter observations suggest that PPDs contain dust grains with various sizes (Acke et al. 2004; Pascual et al. 2016; Davies et al. 2018). The dust size distribution and its variation have considerable effects on disk heating and the resulting mass-loss rate. Small grains have large surface areas per mass, and thus

\mathcal{D}	L_X [ergs $^{-1}$]	\dot{M} [$10^{-9} M_\odot \text{yr}^{-1}$]
10^{-2}	2.5×10^{31}	5.2
10^{-2}	2.5×10^{30}	2.7
10^{-2}	2.5×10^{29}	2.5
10^{-6}	2.5×10^{31}	1.6
10^{-6}	2.5×10^{30}	0.62
10^{-6}	2.5×10^{29}	0.5

Table 1. The mass-loss rates in the runs with different \mathcal{D} and L_X .

contribute predominantly to the net photoelectric heating. If a PPD achieves a state deficient in small dust grains, it is less susceptible to FUV photoelectric heating.

Hutchison et al. (2016) show that the dust size differs between wind regions and the disk region because small dust grains with a few μm diameter are entrained by photoevaporating flows. We have shown that the mass-loss profile is largely determined by the heating at the disk surface, and thus it is unlikely that the dust transportation by photoevaporating flows affect the mass-loss rate. However, mixing of gas and dust near the base may be a complicated process, and thus ideally detailed hydrodynamics simulations with explicit treatment of dust size evolution and dynamical gas-dust (de)coupling would be needed to fully address this issue.

4.2. X-ray Luminosity Dependence

Recent observations suggest that EUV, FUV, X-ray luminosities differ considerably even among the same spectral-type stars (Gullbring et al. 1998; Flaccomio et al. 2003; France et al. 2012; Vidotto et al. 2014; France et al. 2018). Kunitomo et al. (2021) consider the variation of the emissivity of the high-energy radiation together with stellar evolution. For example, for a central star with mass $M_* \geq 1.5 M_\odot$, the X-ray luminosity decreases by a factor of $\sim 10^4$ at the age of 1–10 Myr. To examine the impact of X-ray radiation, we perform an additional set of photoevaporation simulations with varying X-ray luminosities to $L_X = 2.51 \times 10^{29} \text{ergs}^{-1}$ and $L_X = 2.51 \times 10^{31} \text{ergs}^{-1}$, which are 0.1 and 10 times our fiducial value, $L_{X,f}$, respectively. We keep the stellar mass to $M_* = 1 M_\odot$ and the dust-to-gas mass ratio to $\mathcal{D} = 10^{-2}, 10^{-6}$.

The resulting mass-loss rates are listed in Table 1. In the low X-ray cases, H_2 pumping dominantly heats the gas throughout the neutral regions even at the outer radii $r \geq 10r_g$. The temperature structure does not differ from the fiducial run. The disk mass-loss rate does not sensitively depend on L_X , yielding only a factor of a few enhancement by orders-of-magnitude increase of

L_X . This insensitivity indicates that both H_2 pumping and X-ray radiation contribute to the photoevaporation in the low \mathcal{D} cases.

4.3. PPDs where H_2 pumping is important

Earlier in Komaki et al. (2021), we performed a large set of PPD simulations with varying the central stellar mass from $M_* = 1 M_\odot$ to $M_* = 7 M_\odot$. More massive stars with higher UV luminosities generate stronger photoevaporative flows. We expect that H_2 pumping heats the gas at the disk surface to further promote photoevaporation around massive stars. We have run an additional simulation with $M_* = 7 M_\odot$ to examine the effect of H_2 pumping on a disk around a massive star. We set the dust-to-gas mass ratio to the fiducial value of $\mathcal{D} = 10^{-2}$. The simulation yields a mass-loss rate of $\dot{M} = 5.9 \times 10^{-7} M_\odot \text{yr}^{-1}$. We find that the mass-loss rate is twice larger than in the run without H_2 pumping. The base is heated by both FUV photoelectric effect and H_2 pumping, to generate strong outflows.

Finally, we discuss the effect of H_2 pumping in an extremely metal/dust-poor disk. It is relevant to an interesting question regarding the effect of H_2 pumping on the dispersal of primordial-gas disks. Our simulation with $\mathcal{D} = 10^{-8}$ can be regarded as almost a primordial-gas case (Figure 2). The result shows that a primordial disk around a low-mass star is heated by H_2 pumping and X-ray radiation and loses its gas mass by photoevaporation at a rate of $\sim 5 \times 10^{-10} M_\odot \text{yr}^{-1}$. In our future study (Komaki et al., in preparation), we examine the structure, stability and the dispersal of primordial-gas disks.

5. SUMMARY

Recent millimeter observations suggest that the dust amount in a PPD decreases with disk evolution. Although the gas mass is uncertain, the dust abundance and its long-term variation may be important in the process of disk photoevaporation and thereby planet formation in terms of disk dispersal. In the present paper, we have performed a set of radiation-hydrodynamics simulations with varying the dust-to-gas mass ratio to quantify how the effects of H_2 pumping on the photoevaporation of dust-deficient disks. In the standard case with $M_* = 1 M_\odot$ and $\mathcal{D} = 10^{-2}$, H_2 pumping heats the evaporating gas driven by FUV photoelectric heating. H_2 pumping does, therefore, not directly contribute to the mass loss but only affects the temperature structure of the outflow. However, we have also shown that H_2 pumping heating is effective at the inner region within several gravitational radii where the density is higher than the critical density for collisional de-excitation of H_2 molecules.

In relatively dust-rich cases with $\mathcal{D} \geq 10^{-3}$, the disks are heated mainly by the FUV photoelectric process, and the outer molecular region evaporates efficiently. In the other, dust-deficient disks with $\mathcal{D} \leq 10^{-3}$, the dominant heating process is H_2 pumping and X-ray. Since the dust amount can vary on a long timescale as the disk evolves, the temperature structure, the mass-loss profile, and the chemical composition would also change. In future work, we shall study the long-term dispersal process of a PPD by incorporating the formation, growth, and destruction of dust grains.

ACKNOWLEDGMENTS

R.N. acknowledges support from the Special Postdoctoral Researcher program at RIKEN and from Grant-in-Aid for Research Activity Start-up (19K23469). R.K. acknowledges financial support via the Emmy Noether and Heisenberg Research Grants funded by the German Research Foundation (DFG) under grant no. KU 2849/3 and 2849/9. Numerical computations were carried out on Cray XC50 at Center for Computational Astrophysics, National Astronomical Observatory of Japan.

REFERENCES

- Acke, B., van den Ancker, M. E., Dullemond, C. P., van Boekel, R., & Waters, L. B. F. M. 2004, *A&A*, 422, 621, doi: [10.1051/0004-6361:20040197](https://doi.org/10.1051/0004-6361:20040197)
- Alexander, R. D., Clarke, C. J., & Pringle, J. E. 2006, *MNRAS*, 369, 229, doi: [10.1111/j.1365-2966.2006.10294.x](https://doi.org/10.1111/j.1365-2966.2006.10294.x)
- Andrews, S. M., & Williams, J. P. 2005, *ApJ*, 631, 1134, doi: [10.1086/432712](https://doi.org/10.1086/432712)
- Anninos, P., Zhang, Y., Abel, T., & Norman, M. L. 1997, *NewA*, 2, 209, doi: [10.1016/S1384-1076\(97\)00009-2](https://doi.org/10.1016/S1384-1076(97)00009-2)
- Ansdell, M., Williams, J. P., Manara, C. F., et al. 2017, *AJ*, 153, 240, doi: [10.3847/1538-3881/aa69c0](https://doi.org/10.3847/1538-3881/aa69c0)
- Ansdell, M., Williams, J. P., van der Marel, N., et al. 2016, *ApJ*, 828, 46, doi: [10.3847/0004-637X/828/1/46](https://doi.org/10.3847/0004-637X/828/1/46)
- Ansdell, M., Williams, J. P., Trapman, L., et al. 2018, *ApJ*, 859, 21, doi: [10.3847/1538-4357/aab890](https://doi.org/10.3847/1538-4357/aab890)
- Bakes, E. L. O., & Tielens, A. G. G. M. 1994, *ApJ*, 427, 822, doi: [10.1086/174188](https://doi.org/10.1086/174188)
- Bayo, A., Barrado, D., Huélamo, N., et al. 2012, *A&A*, 547, A80, doi: [10.1051/0004-6361/201219374](https://doi.org/10.1051/0004-6361/201219374)
- Clarke, C. J., Gendrin, A., & Sotomayor, M. 2001, *MNRAS*, 328, 485, doi: [10.1046/j.1365-8711.2001.04891.x](https://doi.org/10.1046/j.1365-8711.2001.04891.x)
- D'Alessio, P., Calvet, N., Hartmann, L., Franco-Hernández, R., & Servín, H. 2006, *ApJ*, 638, 314, doi: [10.1086/498861](https://doi.org/10.1086/498861)
- D'Alessio, P., Calvet, N., Hartmann, L., Lizano, S., & Cantó, J. 1999, *ApJ*, 527, 893, doi: [10.1086/308103](https://doi.org/10.1086/308103)
- Davies, C. L., Kraus, S., Harries, T. J., et al. 2018, *ApJ*, 866, 23, doi: [10.3847/1538-4357/aade51](https://doi.org/10.3847/1538-4357/aade51)
- de Gregorio-Monsalvo, I., Ménard, F., Dent, W., et al. 2013, *A&A*, 557, A133, doi: [10.1051/0004-6361/201321603](https://doi.org/10.1051/0004-6361/201321603)
- Draine, B. T., & Bertoldi, F. 1996, *ApJ*, 468, 269, doi: [10.1086/177689](https://doi.org/10.1086/177689)
- Draine, B. T., & Lee, H. M. 1984, *ApJ*, 285, 89, doi: [10.1086/162480](https://doi.org/10.1086/162480)
- Ercolano, B., Clarke, C. J., & Drake, J. J. 2009, *ApJ*, 699, 1639, doi: [10.1088/0004-637X/699/2/1639](https://doi.org/10.1088/0004-637X/699/2/1639)
- Flaccomio, E., Damiani, F., Micela, G., et al. 2003, *ApJ*, 582, 398, doi: [10.1086/344536](https://doi.org/10.1086/344536)
- Font, A. S., McCarthy, I. G., Johnstone, D., & Ballantyne, D. R. 2004, *ApJ*, 607, 890, doi: [10.1086/383518](https://doi.org/10.1086/383518)
- France, K., Arulanantham, N., Fossati, L., et al. 2018, *ApJS*, 239, 16, doi: [10.3847/1538-4365/aae1a3](https://doi.org/10.3847/1538-4365/aae1a3)
- France, K., Schindhelm, E., Herczeg, G. J., et al. 2012, *ApJ*, 756, 171, doi: [10.1088/0004-637X/756/2/171](https://doi.org/10.1088/0004-637X/756/2/171)
- Galli, D., & Palla, F. 1998, *A&A*, 335, 403, <https://arxiv.org/abs/astro-ph/9803315>
- Gorti, U., & Hollenbach, D. 2009, *ApJ*, 690, 1539, doi: [10.1088/0004-637X/690/2/1539](https://doi.org/10.1088/0004-637X/690/2/1539)
- Gorti, U., Hollenbach, D., & Dullemond, C. P. 2015, *ApJ*, 804, 29, doi: [10.1088/0004-637X/804/1/29](https://doi.org/10.1088/0004-637X/804/1/29)
- Grant, S. L., Espaillat, C. C., Megeath, S. T., et al. 2018, *ApJ*, 863, 13, doi: [10.3847/1538-4357/aacda7](https://doi.org/10.3847/1538-4357/aacda7)
- Gressel, O., Ramsey, J. P., Brinch, C., et al. 2020, *ApJ*, 896, 126, doi: [10.3847/1538-4357/ab91b7](https://doi.org/10.3847/1538-4357/ab91b7)
- Gullbring, E., Hartmann, L., Briceño, C., & Calvet, N. 1998, *ApJ*, 492, 323, doi: [10.1086/305032](https://doi.org/10.1086/305032)
- Haisch, Karl E., J., Lada, E. A., & Lada, C. J. 2001, *ApJL*, 553, L153, doi: [10.1086/320685](https://doi.org/10.1086/320685)
- Herczeg, G. J., Wood, B. E., Linsky, J. L., Valenti, J. A., & Johns-Krull, C. M. 2004, *ApJ*, 607, 369, doi: [10.1086/383340](https://doi.org/10.1086/383340)
- Hernández, J., Hartmann, L., Megeath, T., et al. 2007, *ApJ*, 662, 1067, doi: [10.1086/513735](https://doi.org/10.1086/513735)
- Hollenbach, D., & McKee, C. F. 1989, *ApJ*, 342, 306, doi: [10.1086/167595](https://doi.org/10.1086/167595)
- Hutchison, M. A., Laibe, G., & Maddison, S. T. 2016, *MNRAS*, 463, 2725, doi: [10.1093/mnras/stw2191](https://doi.org/10.1093/mnras/stw2191)
- Johnston, K. G., Hoare, M. G., Beuther, H., et al. 2020, *ApJ*, 896, 35, doi: [10.3847/1538-4357/ab8adc](https://doi.org/10.3847/1538-4357/ab8adc)
- Komaki, A., Nakatani, R., & Yoshida, N. 2021, *ApJ*, 910, 51, doi: [10.3847/1538-4357/abe2af](https://doi.org/10.3847/1538-4357/abe2af)

- Kuiper, R., Klahr, H., Dullemond, C., Kley, W., & Henning, T. 2010, *A&A*, 511, A81, doi: [10.1051/0004-6361/200912355](https://doi.org/10.1051/0004-6361/200912355)
- Kuiper, R., & Klessen, R. S. 2013, *A&A*, 555, A7, doi: [10.1051/0004-6361/201321404](https://doi.org/10.1051/0004-6361/201321404)
- Kuiper, R., Yorke, H. W., & Mignone, A. 2020, *ApJS*, 250, 13, doi: [10.3847/1538-4365/ab9a36](https://doi.org/10.3847/1538-4365/ab9a36)
- Kunitomo, M., Ida, S., Takeuchi, T., et al. 2021, *ApJ*, 909, 109, doi: [10.3847/1538-4357/abdb2a](https://doi.org/10.3847/1538-4357/abdb2a)
- Kunitomo, M., Suzuki, T. K., & Inutsuka, S.-i. 2020, *MNRAS*, 492, 3849, doi: [10.1093/mnras/staa087](https://doi.org/10.1093/mnras/staa087)
- Liffman, K. 2003, *PASA*, 20, 337, doi: [10.1071/AS03019](https://doi.org/10.1071/AS03019)
- Mamajek, E. E. 2009, in *American Institute of Physics Conference Series*, Vol. 1158, American Institute of Physics Conference Series, ed. T. Usuda, M. Tamura, & M. Ishii, 3–10, doi: [10.1063/1.3215910](https://doi.org/10.1063/1.3215910)
- Mathews, G. S., Williams, J. P., Ménard, F., et al. 2012, *ApJ*, 745, 23, doi: [10.1088/0004-637X/745/1/23](https://doi.org/10.1088/0004-637X/745/1/23)
- Meyer, M. R., Backman, D. E., Weinberger, A. J., & Wyatt, M. C. 2007, in *Protostars and Planets V*, ed. B. Reipurth, D. Jewitt, & K. Keil, 573. <https://arxiv.org/abs/astro-ph/0606399>
- Mignone, A., Bodo, G., Massaglia, S., et al. 2007, *ApJS*, 170, 228, doi: [10.1086/513316](https://doi.org/10.1086/513316)
- Nakatani, R., Hosokawa, T., Yoshida, N., Nomura, H., & Kuiper, R. 2018a, *ApJ*, 857, 57, doi: [10.3847/1538-4357/aab70b](https://doi.org/10.3847/1538-4357/aab70b)
- . 2018b, *ApJ*, 865, 75, doi: [10.3847/1538-4357/aad9fd](https://doi.org/10.3847/1538-4357/aad9fd)
- Nakatani, R., Kobayashi, H., Kuiper, R., Nomura, H., & Aikawa, Y. 2021, *ApJ*, 915, 90, doi: [10.3847/1538-4357/ac0137](https://doi.org/10.3847/1538-4357/ac0137)
- Nelson, R. P., & Langer, W. D. 1997, *ApJ*, 482, 796, doi: [10.1086/304167](https://doi.org/10.1086/304167)
- Nomura, H., & Millar, T. J. 2005, *A&A*, 438, 923, doi: [10.1051/0004-6361:20052809](https://doi.org/10.1051/0004-6361:20052809)
- Omukai, K., Hosokawa, T., & Yoshida, N. 2010, *ApJ*, 722, 1793, doi: [10.1088/0004-637X/722/2/1793](https://doi.org/10.1088/0004-637X/722/2/1793)
- Osterbrock, D. E. 1989, *Astrophysics of gaseous nebulae and active galactic nuclei* (University Science Books)
- Owen, J. E., Ercolano, B., Clarke, C. J., & Alexander, R. D. 2010, *MNRAS*, 401, 1415, doi: [10.1111/j.1365-2966.2009.15771.x](https://doi.org/10.1111/j.1365-2966.2009.15771.x)
- Pascual, N., Montesinos, B., Meeus, G., et al. 2016, *A&A*, 586, A6, doi: [10.1051/0004-6361/201526605](https://doi.org/10.1051/0004-6361/201526605)
- Pascucci, I., Testi, L., Herczeg, G. J., et al. 2016, *ApJ*, 831, 125, doi: [10.3847/0004-637X/831/2/125](https://doi.org/10.3847/0004-637X/831/2/125)
- Pollack, J. B., Hollenbach, D., Beckwith, S., et al. 1994, *ApJ*, 421, 615, doi: [10.1086/173677](https://doi.org/10.1086/173677)
- Ribas, Á., Merín, B., Bouy, H., & Maud, L. T. 2014, *A&A*, 561, A54, doi: [10.1051/0004-6361/201322597](https://doi.org/10.1051/0004-6361/201322597)
- Richling, S., & Yorke, H. W. 2000, *ApJ*, 539, 258, doi: [10.1086/309198](https://doi.org/10.1086/309198)
- Röllig, M., Ossenkopf, V., Jeyakumar, S., Stutzki, J., & Sternberg, A. 2006, *A&A*, 451, 917, doi: [10.1051/0004-6361:20053845](https://doi.org/10.1051/0004-6361:20053845)
- Santoro, F., & Shull, J. M. 2006, *ApJ*, 643, 26, doi: [10.1086/501518](https://doi.org/10.1086/501518)
- Schindhelm, E., France, K., Herczeg, G. J., et al. 2012, *ApJL*, 756, L23, doi: [10.1088/2041-8205/756/1/L23](https://doi.org/10.1088/2041-8205/756/1/L23)
- Spitzer, L. 1978, *Physical processes in the interstellar medium* (Wiley-Interscience), doi: [10.1002/9783527617722](https://doi.org/10.1002/9783527617722)
- Suzuki, T. K., Ogihara, M., Morbidelli, A. r., Crida, A., & Guillot, T. 2016, *A&A*, 596, A74, doi: [10.1051/0004-6361/201628955](https://doi.org/10.1051/0004-6361/201628955)
- Tielens, A. G. G. M., & Hollenbach, D. 1985, *ApJ*, 291, 747, doi: [10.1086/163112](https://doi.org/10.1086/163112)
- Vidotto, A. A., Gregory, S. G., Jardine, M., et al. 2014, *MNRAS*, 441, 2361, doi: [10.1093/mnras/stu728](https://doi.org/10.1093/mnras/stu728)
- Walsh, C., Nomura, H., & van Dishoeck, E. 2015, *A&A*, 582, A88, doi: [10.1051/0004-6361/201526751](https://doi.org/10.1051/0004-6361/201526751)
- Wang, L., & Goodman, J. 2017, *ApJ*, 847, 11, doi: [10.3847/1538-4357/aa8726](https://doi.org/10.3847/1538-4357/aa8726)
- Yorke, H. W., & Welz, A. 1996, *A&A*, 315, 555